






REPORT

Extramitochondrial cardiolipin suggests a novel function of mitochondria in spermatogenesis

Mindong Ren^{1,2}, Yang Xu¹, Hediye Erdjument-Bromage^{3,4} , Alec Donelian¹, Colin K.L. Phoon⁵ , Naohiro Terada⁶, Douglas Strathdee⁷ , Thomas A. Neubert^{3,4} , and Michael Schlame^{1,2} 

Mitochondria contain cardiolipin (CL), an organelle-specific phospholipid that carries four fatty acids with a strong preference for unsaturated chains. Unsaturation is essential for the stability and for the function of mitochondrial CL. Surprisingly, we found tetrapalmitoyl-CL (TPCL), a fully saturated species, in the testes of humans and mice. TPCL was absent from other mouse tissues but was the most abundant CL species in testicular germ cells. Most intriguingly, TPCL was not localized in mitochondria but was in other cellular membranes even though mitochondrial CL was the substrate from which TPCL was synthesized. During spermiogenesis, TPCL became associated with the acrosome, a sperm-specific organelle, along with a subset of authentic mitochondrial proteins, including Ant4, Suox, and Spata18. Our data suggest that mitochondria-derived membranes are assembled into the acrosome, challenging the concept that this organelle is strictly derived from the Golgi apparatus and revealing a novel function of mitochondria.

Introduction

Cardiolipin (CL) has been recognized as mitochondria's "own" phospholipid. It is intimately associated with proteins of the inner mitochondrial membrane (Beyer and Klingenberg, 1985) and strongly supports the clustering of protein complexes to supercomplexes (Zhang et al., 2002; Mileykovskaya and Dowhan, 2014). Lack of CL causes severe mitochondrial dysfunction in yeast (Jiang et al., 2000) and in *Drosophila melanogaster* (Acehan et al., 2011) and leads to early embryonic lethality in mice (Zhang et al., 2011). In humans, CL deficiency is associated with Barth syndrome, a systemic disease involving heart and skeletal muscles (Clarke et al., 2013).

CL is rich in unsaturated fatty acids, which are essential for the function of CL in mitochondria (Ren et al., 2014; Lu and Claypool, 2015). This is best exemplified in Barth syndrome where mutations in tafazzin (TAZ) cause a moderate increase in the fatty acid saturation specifically in CL. This leads to CL degradation, which in turn has a destabilizing effect on the supercomplexes of oxidative phosphorylation (Xu et al., 2016). Given the importance of unsaturated fatty acids for the function of CL, it was highly unexpected when fully saturated tetrapalmitoyl-CL (TPCL) was first discovered in the testes of rats (Wang et al., 2007).

Here, we confirm the presence of TPCL in the testes of humans and mice, suggesting that it is a widespread phenomenon. This raises questions, such as which cell type is TPCL associated with and what is its function? TPCL is strikingly different from unsaturated CL because the latter is one of the most fluid phospholipids whereas the former remains in the gel phase at body temperature (Lewis and McElhaney, 2009). Therefore, TPCL is expected to segregate from unsaturated CL, which makes it difficult to conceptualize how the two lipids can coexist in mitochondrial membranes.

Results and discussion

Testicular germ cells contain a fully saturated CL species

Following up on the discovery of TPCL in rat testes (Wang et al., 2007), we analyzed the CL composition of testes from humans and mice, where we confirmed the presence of TPCL (Fig. S1 a). Since fully saturated CL is rather improbable given the established unsaturation of mitochondrial lipids (Horvath and Daum, 2013), we first verified its identity by multistage mass spectrometry (MSn). Our measurements corroborated the structure of a CL molecule with four palmitoyl residues (Fig. S1 b). TPCL

¹Department of Anesthesiology, New York University School of Medicine, New York, NY; ²Department of Cell Biology, New York University School of Medicine, New York, NY; ³Kimmel Center for Biology and Medicine at the Skirball Institute, New York University School of Medicine, New York, NY; ⁴Department of Biochemistry and Molecular Pharmacology, New York University School of Medicine, New York, NY; ⁵Department of Pediatrics, New York University School of Medicine, New York, NY; ⁶Department of Pathology, University of Florida College of Medicine, Gainesville, FL; ⁷Transgenic Technology Laboratory, Cancer Research UK Beatson Institute, Glasgow, UK.

Correspondence to Mindong Ren: mindong.ren@nyumc.org; Michael Schlame: michael.schlame@med.nyu.edu.

© 2019 Ren et al. This article is distributed under the terms of an Attribution-Noncommercial-Share Alike-No Mirror Sites license for the first six months after the publication date (see <http://www.rupress.org/terms/>). After six months it is available under a Creative Commons License (Attribution-Noncommercial-Share Alike 4.0 International license, as described at <https://creativecommons.org/licenses/by-nc-sa/4.0/>).

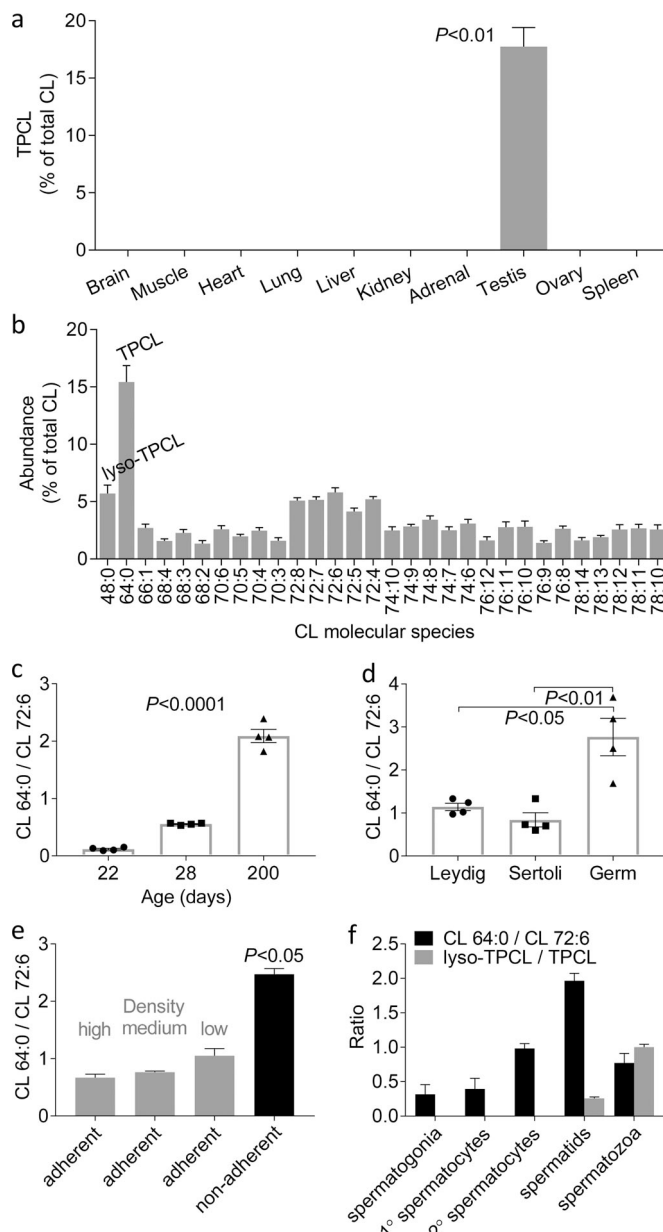


Figure 1. Testicular germ cells contain TPCL. Lipids were extracted from wild-type mouse (C57BL/6) tissues and cells. CL was analyzed by MALDI-TOF MS. (a) Adult mouse tissues. (b) Adult mouse testes. (c) Mouse testes at different ages. (d) Crude testicular cell populations. (e) Different germ cell populations (maturity increases from left to right). (f) Germ cells separated by flow cytometry. Data are mean values \pm SEMs (a: $n = 3$; b: $n = 8$; c–f: $n = 4$). Mean values were compared by Student's *t* test (a, d, e) and by ANOVA (c).

was only present in testes and not in other mouse tissues (Fig. 1 a), but in testes it was more abundant than any of the “regular” CL species (Fig. 1 b).

Interestingly, TPCL emerged only after the third week of life (Fig. 1 c), an age in which the first wave of spermatogenesis has advanced to the post-meiotic stage. This implicated germ cell development and raised the question as to which cell type involved in the reproductive process was the source of TPCL. After separating testes into three crude fractions enriched in Leydig, Sertoli, and germ cells (Chang et al., 2011), we found TPCL to be

most abundant in the germ cells (Fig. 1 d). Further purification based on tissue adhesion and density revealed that the purest and most mature germ cells contained the highest proportion of TPCL (Fig. 1 e). Finally, we separated germ cells by flow cytometry into spermatogonia, spermatocytes, and spermatids (Fig. S2) and determined that the concentration of TPCL increased along the developmental pathway up to the spermatid stage (Fig. 1 f). Mature sperm, isolated separately from the epididymis, also contained TPCL, albeit in a lower quantity than spermatids, apparently due to its degradation to lyso-TPCL (Fig. 1, b and f; and Fig. S1 b). Thus, TPCL originated with germ cells, rose sharply during meiosis, and partially degraded in the post-meiotic phase.

Saturated CL is located in the acrosome

Surprisingly, TPCL did not mimic the subcellular distribution of other CL species. Whereas “typical” CLs like CL 72:6 and CL 72:4 followed mitochondrial marker proteins, as expected, TPCL corresponded more closely to markers of the Golgi apparatus (receptor-binding cancer antigen 1) and the endoplasmic reticulum (protein disulfide isomerase).¹ TPCL behaved similarly to other saturated lipids, such as sphingomyelin (SM d18:1/16:0) and dipalmitoyl-phosphatidylinositol (PI 16:0/16:0) but differed from polyunsaturated PI 18:0/20:4 (Fig. 2 a). We speculated that TPCL and unsaturated CL might be associated with distinct types of mitochondria because germ cells carry two fundamentally different forms referred to as “orthodox” and as “condensed” (De Martino et al., 1979; Meinhardt et al., 1999; Ramalho-Santos and Amaral, 2013). Indeed, we found more TPCL in fraction 8L, in which $86 \pm 19\%$ of mitochondria were condensed, than in fraction 8H, in which only $30 \pm 8\%$ of mitochondria were condensed ($n = 3$; Fig. 2 a). However, when we separated condensed mitochondria from nonmitochondrial membranes by immunoaffinity binding, we recovered TPCL in the nonmitochondrial fraction (Fig. 2 b).

The presence of extra-mitochondrial CL was corroborated by fluorescence microscopy of round spermatids. Specifically, we detected intracellular vesicles that stained with the CL-specific dye nonyl acridine orange (NAO) but not with the mitochondria-specific dye MitoTracker. These vesicles were different from mitochondria that attracted both dyes (Fig. 2 c). In 19 cells, we observed 638 NAO-positive organelles, of which 38 (6.0%) did not stain with MitoTracker. To identify the compartment that carried TPCL, we performed affinity purifications with organelle-specific antibodies but could not find any enrichment of TPCL in endosomes, the endoplasmic reticulum, or the plasma membrane (Table S1). Thus, we turned to spermatozoa, hoping that their polarized distribution of organelles would aid us in identifying the TPCL compartment. As expected, we observed MitoTracker only in the midpiece of sperm, the established localization of mitochondria (Ramalho-Santos and Amaral, 2013). In contrast, the CL-specific dye NAO stained two different locations, namely the midpiece and the head, strongly suggesting the presence of extra-mitochondrial

¹Lipids are identified by an x:y code, in which x represents the number of carbon atoms and y the number of double bonds.

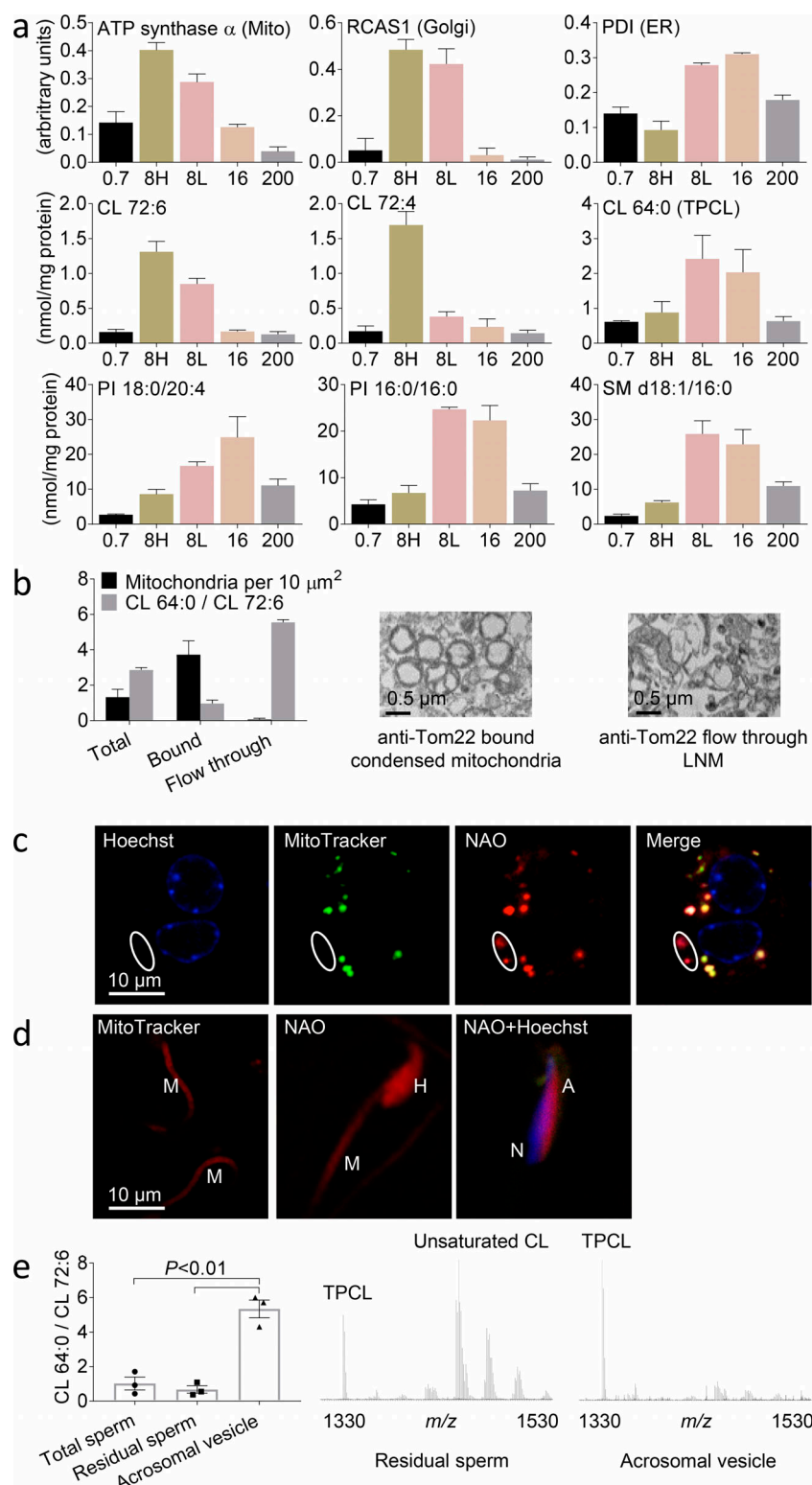


Figure 2. TPCL is associated with the acrosome. (a)

Subcellular fractions were prepared from wild-type mouse (C57BL/6) testis homogenate by centrifugation at 700 g (0.7), 8,000 g (8), 16,000 g (16), and 200,000 g (200). The 8,000-g pellet was separated into a high-density (8H) and a low-density (8L) fraction by Percoll gradient. Fractions were analyzed for organelle markers by quantitative Western blotting and for lipids by MS. **(b)** Fraction 8L was loaded onto an affinity column linked to the anti-Tom22 antibody. The bound fraction (condensed mitochondria) and the flow-through fraction (LNMs) were analyzed by MS and by EM. **(c)** Two round spermatids were stained with Hoechst (nuclei), MitoTracker (mitochondria), and NAO (CL) and analyzed by fluorescence microscopy. The encircled organelles stained with NAO but not with MitoTracker. **(d)** Sperm were stained with the indicated dyes and analyzed by fluorescence microscopy. Mitotracker stained the mid-piece (M); NAO stained both the midpiece and the head (H). In the head, the nucleus (N) can be distinguished from the acrosome (A). **(e)** The acrosome reaction was induced in isolated sperm. Cells were separated from the released vesicles and analyzed by MS. Bar graphs show mean values \pm SEMs ($n = 3$). Mean values were compared by Student's t test. PDI, protein disulfide isomerase; PI, dipalmitoyl-phosphatidylinositol; RCAS1, receptor-binding cancer antigen 1; SM, sphingomyelin.

CL in the sperm head (Fig. 2 d). The shape and the localization of the NAO-positive organelle in the sperm head matched the characteristic appearance of the acrosome (Berruti, 2016). To demonstrate unambiguously whether acrosomes contain TPCL, we released acrosome-plasma membrane vesicles from isolated sperm (Brucker and Lipford, 1995) and analyzed CL by MS. Indeed, acrosomal vesicles contained TPCL but

virtually no unsaturated CL whereas the residual sperm contained mostly unsaturated CL (Fig. 2 e). TPCL copurified with other saturated lipids, including sphingomyelin, the testis-specific seminolipid, and saturated phosphatidylcholine, in detergent-resistant membranes from acrosomal vesicles (Table S2). Hence, we physically separated unsaturated CL from TPCL and have shown that the former is a

constituent of mitochondria but the latter a constituent of lipid rafts in acrosomes.

Acrosomal CL is derived from mitochondria

The presence of TPCL in acrosomes is defying the established notion that CL is exclusively present in mitochondria (Ren et al., 2014). Although there have been rare reports of extramitochondrial CL in the peroxisomes of yeast (Zinser et al., 1991; Wriessnegger et al., 2007) and in the plasma membrane of apoptotic cells (Sorice et al., 2000, 2004), their significance has remained unclear. To identify the compartment in which CL is synthesized, we determined the distribution of CL synthase among subcellular fractions. Its activity corresponded closely to the distribution of mitochondria rather than the distribution of TPCL. Importantly, the membranes that carried TPCL (light nonmitochondrial membranes [LNMs]) did not contain any CL synthase activity, suggesting that TPCL was derived from mitochondria (Fig. 3 a). If mitochondrial CL is indeed the substrate of TPCL, it must undergo acyl remodeling in order to replace the mostly unsaturated fatty acids of mitochondrial CL with palmitate. In support of this notion, we observed the expected remodeling intermediates, i.e., CL species with one to three palmitoyl residues (Fig. 3 b and Table S3). To further scrutinize the mitochondrial origin of TPCL, we perturbed the CL homeostasis of mitochondria by deleting TAZ, the mitochondrial enzyme that is responsible for the high unsaturation of CL (Vreken et al., 2000) and for its stability (Xu et al., 2016). As expected, TAZ knockout (KO) stimulated CL degradation to monolyso-CL and altered the molecular composition of CL in favor of saturated fatty acids. But despite the increase in partially saturated species, TAZ KO nearly abolished the formation of TPCL (Fig. 3, c and d). These data indicate that the mitochondrial homeostasis of CL is crucial for TPCL production and thus affirm the mitochondrial origin of TPCL.

TAZ KO not only prevented the formation of TPCL but it also inhibited germ cell meiosis as demonstrated by the reduced abundance of round spermatids and the near absence of elongated spermatids (Fig. 3, e and f). Our results confirm previously published data in TAZ-deficient chimeras (Cadaltbert et al., 2015) and underscore the importance of mitochondria for germ cell development. It has been shown that germ cells contain a unique form of mitochondria, referred to as condensed, in which the matrix is reduced to a narrow capsule around a lone spherical crista (Fig. 3 g; De Martino et al., 1979). The transition from orthodox to condensed mitochondria occurs through an intermediate form in the prophase of meiosis. After that, condensed mitochondria become the most abundant type until they gradually disappear in the post-meiotic phase (De Martino et al., 1979; Meinhardt et al., 1999). We confirmed that condensed mitochondria were the most abundant form in normal spermatocytes but were replaced by orthodox and intermediate mitochondria in spermatids (Fig. 3, g and h). TAZ KO induced a striking increase in orthodox mitochondria in all germ cells and a reduction of condensed mitochondria in spermatocytes, suggesting that TAZ KO inhibited the mitochondrial transformation during early meiosis (Fig. 3 h). In summary, we have shown that TAZ KO impairs the transformation from orthodox to condensed

mitochondria, prevents the synthesis of TPCL, and blocks the progression of germ cells into the spermatid stage. These data suggest that an abnormal CL metabolism is sufficient to impede the biogenesis of condensed mitochondria and that the CL of condensed mitochondria is the substrate for the synthesis of TPCL. Consistent with that, we found the direct precursors of TPCL (tripalmitoyl-CLs) only in condensed and not in orthodox mitochondria (Fig. 3 b).

Mitochondrial proteins are present in the acrosome

Since little is known about the function of condensed mitochondria, we compared the proteomes of orthodox and condensed mitochondria by tandem mass tag (TMT) technology combined with liquid chromatography-MS (LC-MS; Huang et al., 2017). Proteins that were more abundant in orthodox than in condensed mitochondria belonged mostly to the matrix compartment whereas proteins that were more abundant in condensed than in orthodox mitochondria belonged mostly to the outer membrane and to the intermembrane space (Fig. 4 a). This is consistent with the relative volumes of the matrix and the intermembrane space in orthodox and in condensed mitochondria, respectively.

Among the proteins enriched in condensed mitochondria were three testis-specific proteins, including the sperm mitochondrial-associated cysteine-rich protein (Smcp), the testis-specific cytochrome c (Cyt), and the adenine nucleotide translocase 4 (Ant4; Fig. 4 a). The function of these proteins has remained enigmatic. In particular, Ant4, the most abundant member of the condensed mitochondrial proteome, has been shown to exchange ADP and ATP across lipid bilayers (Dolce et al., 2005) and to be essential for spermatogenesis (Brower et al., 2009), but it is not clear why germ cells require a specific isoform of the ADP-ATP translocase in addition to the ubiquitous Ant1 and Ant2 (Lim et al., 2015). Surprisingly, when we analyzed the location of Ant4 in sperm by immunofluorescence (Rodić et al., 2005), we observed it not only in the midpiece where mitochondria are located but also in the head where it colocalized with the acrosomal marker Izumol (Fig. 4 b). Whereas Ant4 was detectable both in the midpiece and the head, respiratory complex II was only present in the midpiece, demonstrating that not all mitochondrial proteins are associated with the acrosome (Fig. 4 b).

This prompted us to investigate whether additional mitochondrial proteins can be found in the acrosome. We used TMT analysis to compare the proteome of testis mitochondria with the proteome of acrosomal vesicles released from sperm. As expected, the acrosome/mitochondria abundance ratio was low for most proteins with mitochondrial annotation. However, we identified 10 mitochondrial proteins with an abnormally high acrosome/mitochondria abundance ratio, indicative of an acrosomal localization. Among those, five proteins were specifically associated with condensed mitochondria (Fig. S3 a). We selected two of those proteins for further analysis by immunofluorescence because of the availability of antibodies. They included Spata 18, also known as a mitochondria-eating protein that orchestrates the degradation of unhealthy mitochondria (Kitamura et al., 2011; Tsuneki et al., 2015), and Suox, the

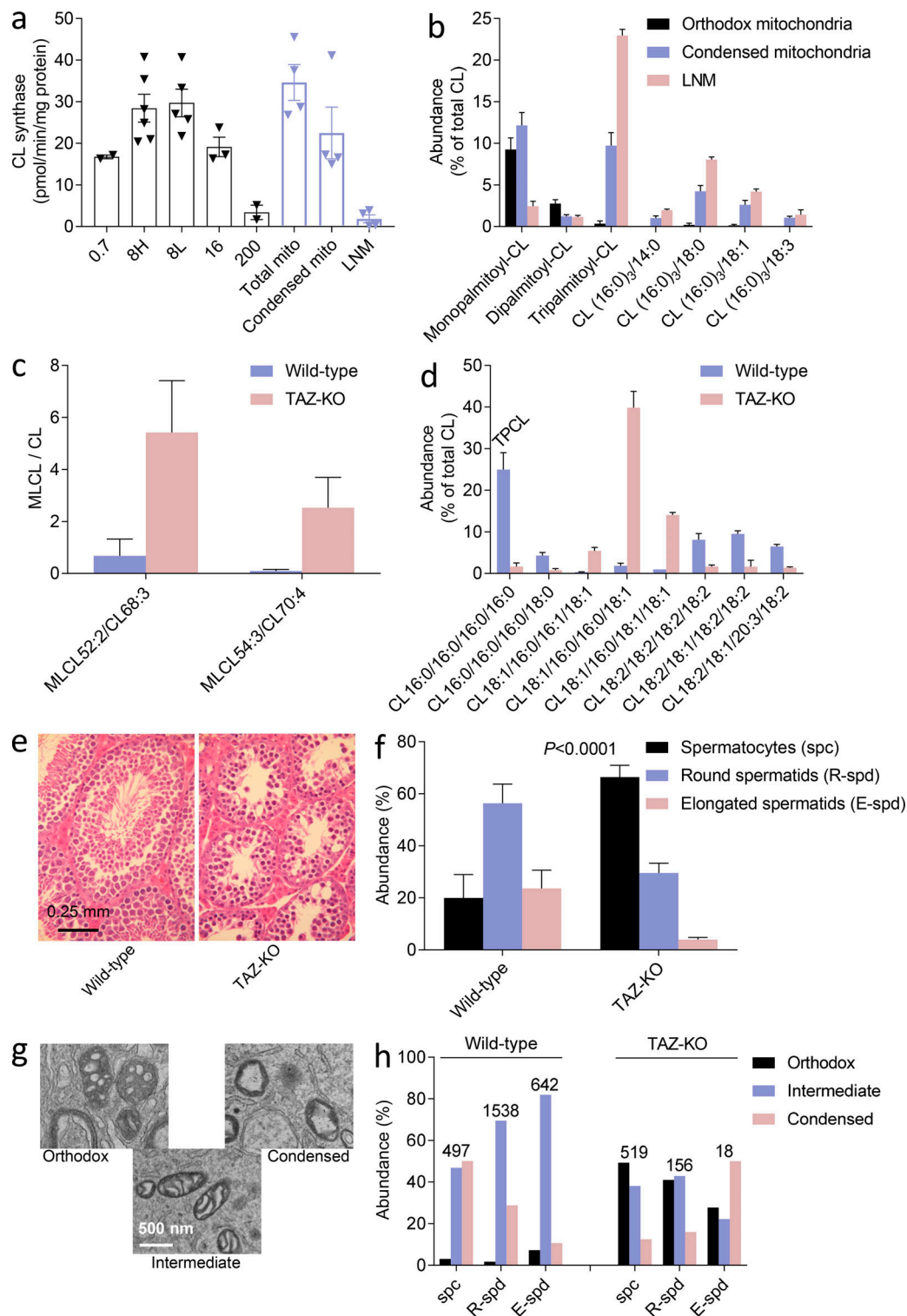


Figure 3. TPCL is formed from CL of condensed mitochondria. (a) Subcellular fractions were prepared from testis homogenate as shown in Fig. 2 a, and CL synthase activity was measured. (b) Orthodox and condensed mitochondria were separated by Percoll density gradient centrifugation and affinity-purified with the Tom22 antibody. LNMs were recovered from the anti-Tom22 flow through of condensed mitochondria. CL was analyzed by LC-MS/MS. Bar graphs show mean values \pm SEMs ($n = 3$). (c and d) CL and monolysophosphatidylcholine (MLCL) from whole testes were analyzed by LC-MS/MS. Bar graphs show mean values \pm SEMs ($n = 3$). (e) Histological sections showing the seminiferous tubules of mouse testes were stained with hematoxylin and eosin. (f) The distribution of germ cell types was determined in electron micrographs from mouse testes. Bar graphs show mean values \pm SEMs ($n = 3$). Wild-type and TAZ KO were compared by the χ^2 test. (g) Electron micrographs show different categories of mitochondria in normal male germ cells. (h) Orthodox, intermediate, and condensed mitochondria were quantified in different germ cells of mouse testes by using EM. The total number of mitochondria analyzed in each cell type is given on top. The composition of mitochondria was different between wild type and TAZ-KO in each cell type ($P < 0.0001$, χ^2 test).

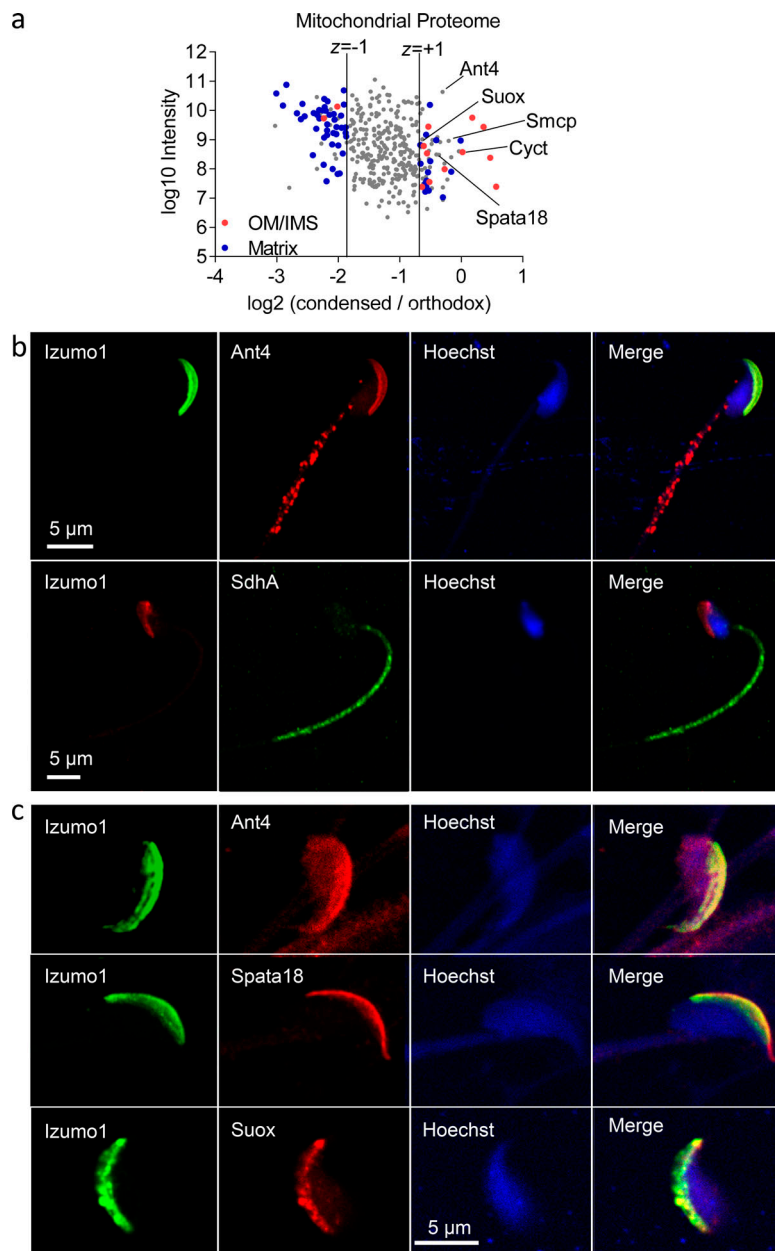


Figure 4. The acrosome contains mitochondrial proteins. (a) Orthodox and condensed mitochondria were separated by density gradient and affinity purified. The organelles were analyzed by TMT proteomics technology. Logarithmic MS1 signal intensities were plotted against the logarithmic ratio of the MS2-based intensities of the condensed tag over the orthodox tag. Only mitochondrial proteins are shown. The data were skewed toward negative log₂ ratios because mitochondrial proteins were relatively underrepresented in condensed mitochondria. Proteins with a z-score less than -1 (specific for orthodox mitochondria) and proteins with a z-score greater than +1 (specific for condensed mitochondria) were analyzed with regard to their submitochondrial localization. OM, outer membrane; IMS, intermembrane space. (b) Sperm were analyzed by immunofluorescence by using commercial antibodies to Izumo1 (acrosome marker), Ant4, and the SdhA subunit of respiratory complex II. Hoechst dye was used to stain the nucleus. (c) Sperm heads were analyzed by immunofluorescence by using antibodies to Izumo1, Ant4, Spata18, and Suox.

mitochondrial sulfite oxidase. Both Spata 18 and Suox immunofluorescence mimicked the characteristic shape of the acrosome in sperm and colocalized with the acrosomal marker Izumo1 (Fig. 4 c). Quantitative Western blot analysis showed that Suox was actually more abundant in acrosomal vesicles than in mitochondria (Fig. S3 b). Thus, we have shown three mitochondrial proteins (Ant4, Suox, and Spata18) and CL to be associated with the acrosome.

Nascent acrosomes acquire mitochondrial proteins during the Golgi phase

The presence of mitochondrial proteins in the acrosome raises questions about their function. For instance, Ant4 is crucial for germ cell meiosis (Brower et al., 2007, 2009) despite the redundant co-expression of other isoforms of the ADP/ATP carrier. We confirmed that ANT4 KO mice did not contain any

spermatids and consequently had testicular atrophy, which was even more severe than in TAZ KO mice (Fig. 5 a). Searching for a mechanism, we found that the ANT4 KO inhibited the transformation of orthodox into condensed mitochondria (Fig. 5 b), which was accompanied by an incomplete contraction of the matrix compartment in >90% of intermediate mitochondria (Fig. 5 c). This suggested a defect in the process of matrix contraction, which is critical for mitochondrial transformation. Furthermore, ANT4 KO caused a complete lack of TPCL and additional alterations in the molecular species composition of mitochondrial CL (Fig. 5 d). Thus, Ant4 is essential for the transition of orthodox into condensed mitochondria, and this transition is necessary to form TPCL, further supporting the important role of condensed mitochondria for the TPCL pathway. Since (1) CL and Ant4 colocalized to acrosomes and mitochondria, (2) acrosomal CL was derived from condensed

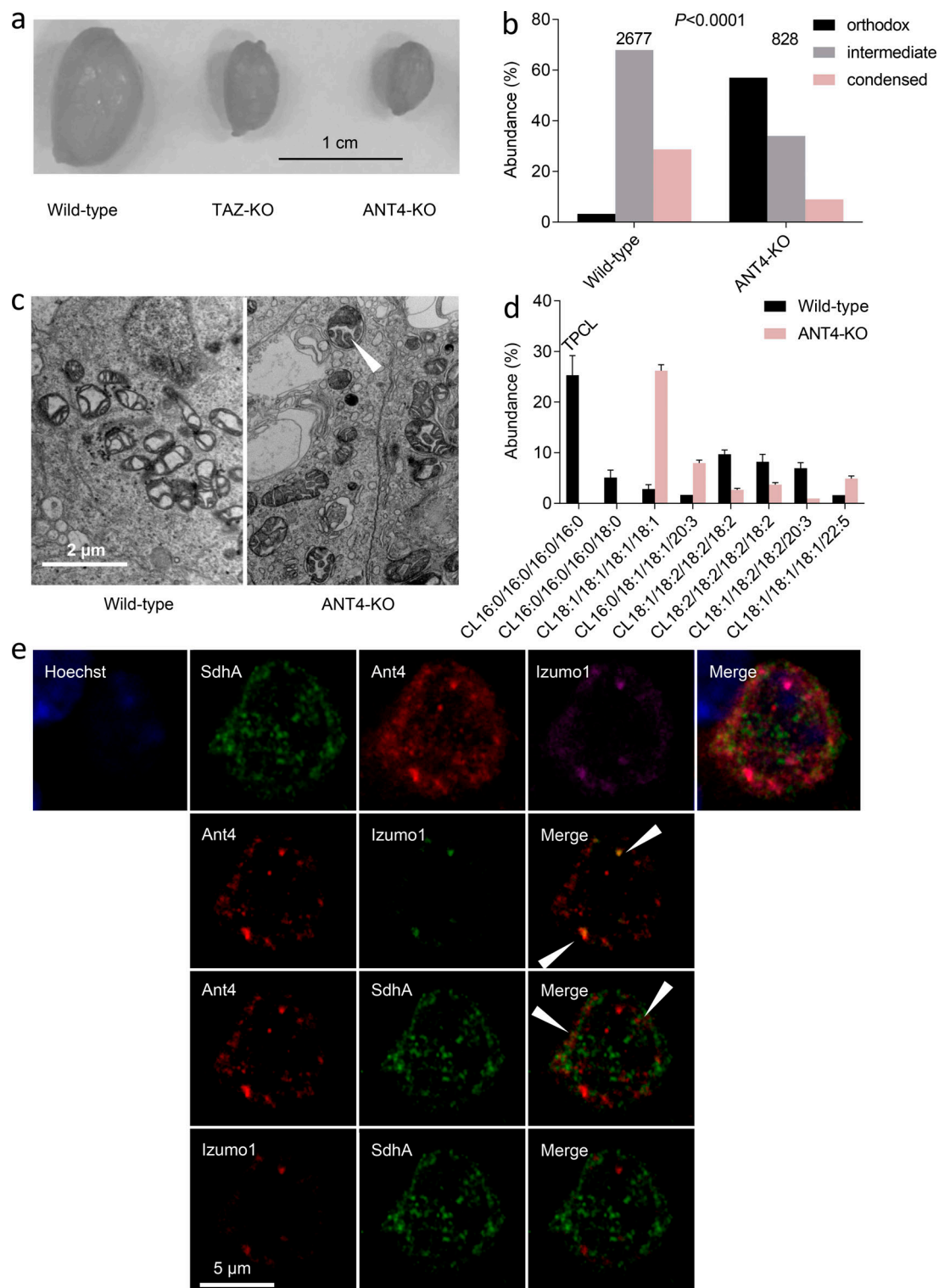


Figure 5. Ant4 is assembled into pro-acrosomal granules. (a) Testes were excised from three mouse models (all in C57BL/6 background). (b) Orthodox, intermediate, and condensed mitochondria were quantified in all germ cells of mouse testes by using EM. The total number of mitochondria analyzed is given on top. The composition of mitochondria in wild type and ANT4-KO was compared by the χ^2 test. (c) Electron micrographs show intermediate mitochondria in mouse spermatocytes. The arrowhead points to a mitochondrion with incomplete contraction of the matrix. (d) Testis CL was analyzed by LC-MS/MS. Bar graphs show mean values \pm SEMs ($n = 3$). (e) Round spermatids were analyzed by immunofluorescence by using antibodies to Ant4, Izumo1 (acrosome marker), and the SdhA subunit of respiratory complex II. The nucleus was stained by Hoechst dye. The top row shows real fluorescence colors for Hoechst, SdhA, and Ant4, and magenta pseudocolor for Izumo1. Other rows show pairs of red/green pseudocolors to identify specific colocalizations. The arrowheads indicate colocalization sites.

mitochondria, and (3) the biogenesis of condensed mitochondria depended on Ant4, it is very likely that acrosomal Ant4 is also derived from condensed mitochondria.

This raises the issue of the mechanism by which Ant4 becomes associated with the acrosome. Acrosomes are formed in four phases, called (1) the Golgi phase in which pro-acrosomal vesicles from the Golgi apparatus coalesce to a single granule, (2) the cap phase in which the granule expands and attaches to the nuclear envelope, (3) the acrosome phase in which the characteristic morphology evolves, and (4) the maturation phase in which the acrosome assumes its final functional state (Berruti, 2016). We found Ant4 to be associated with three compartments in round spermatids, including mitochondria (colocalization with SdhA), pro-acrosomal granules (colocalization with Izumo1), and another structure that contained neither SdhA nor Izumo1 (Fig. 5 e). Our data are consistent with the idea that Ant4-containing mitochondria evolve into Ant4-containing vesicles, which in turn are targeted to the acrosome. The presence of Ant4 in the pro-acrosomal granule tentatively suggests that Ant4 enters the acrosomal compartment during the Golgi phase. Suox and Spata18 immunofluorescence data also supported the targeting of these proteins from mitochondria to pro-acrosomal granules during the Golgi phase (Fig. S4).

Conclusions

In summary, we have discovered a single, fully saturated species of CL in extra-mitochondrial membranes and have shown that it is assembled into the acrosome. This expands the traditional view of CL, which until now has been considered a specific mitochondrial lipid. We also found select mitochondrial proteins in the acrosome, strongly suggesting a role of mitochondria in acrosome formation, and we identified the testis-specific condensed mitochondria as the proximal source of this pathway. Our results reveal a novel function of mitochondria and raise the question of whether there is a wider mitochondrial involvement in building other organelles, either specific to germ cells or to eukaryotic cells in general. For instance, mitochondria have been recognized as the precursor of the nebenkern in insect sperm (Perry et al., 1959), and they have been implicated in the assembly of peroxisomes (Sugiura et al., 2017).

The idea that mitochondria contribute to the biogenesis of acrosomes is new, and a detailed mechanism remains to be established. Acrosomes are thought to be lysosome-related organelles (Raposo et al., 2007) that derive their membranes from the Golgi apparatus and perhaps from early endosomes (Okabe, 2013; Berruti, 2016). Substantial evidence supports the Golgi origin of the vesicles that migrate to the apex of the developing sperm and coalesce into the acrosome (Okabe, 2013; Berruti, 2016). However, our data implicate an additional source, namely condensed mitochondria, even though the contribution that mitochondria make to the acrosome mass seems small. TPCL comprised ~6% of lipids in acrosomal rafts, and the combined intensities of proteins with mitochondrial annotation in the acrosome was only 7% of the proteins with acrosomal annotation. Nevertheless, we believe that mitochondria are important to acrosome biogenesis because both the disturbance of mitochondrial CL (TAZ KO) and the deletion of mitochondrial Ant4

(ANT4 KO) resulted in the inhibition of acrosome formation and in infertility. The actual function of mitochondrial molecules remains to be established, and it is not known whether mitochondrial proteins undergo posttranslational modifications as they are incorporated into acrosomes. Ant4, for instance, belongs to a family of ADP/ATP carriers and has thus been thought to support cellular bioenergetics (Dolce et al., 2005; Kim et al., 2007; Brower et al., 2009), but it may have additional unrecognized activities that come into play after it leaves the mitochondrial compartment.

Materials and methods

Human and murine specimens

A frozen specimen of a human testis was obtained from Pro-teogenex. Mouse protocols were approved by the Institutional Animal Care and Use Committee of New York University School of Medicine. Mice (C57BL/6) were housed under temperature-controlled conditions and a 12-h light/dark cycle with free access to drinking water and food. Unless stated otherwise, mice were sacrificed at the age of 3–4 mo. Mouse testes and epididymis were dissected under anesthesia, after which the animals were sacrificed. Sperm were collected in DMEM from minced epididymis by gentle mechanical agitation for 30 min at 37°C. Sperm were separated from fragments of the epididymis by sedimentation for 2 min. This method yields sperm from the entire epididymis.

Mouse models

Both KO models used in this study were in the C57BL/6 background. The TAZ KO mouse model was developed by D. Strathdee of the Cancer Research UK Beatson Institute. In this model, two loxP sites flank exons 5–10 of the TAZ gene. We obtained floxed sperm in order to generate the KO model by Cre recombination. The ANT4 KO mouse model was developed by the laboratory of N. Terada (Brower et al., 2007). The mouse line was rederived for the purpose of this study by in vitro fertilization of C57BL/6 eggs with sperm from heterozygous (Ant4^{+/-}) males. The heterozygous animals were bred to produce homozygous Ant4 KO mice. Genotyping was performed by PCR analysis of genomic DNA as previously described (Brower et al., 2007).

Isolation of testicular cells from mice

Crude cell populations were isolated from the whole testis as described previously (Chang et al., 2011). In brief, decapsulated testes were digested with collagenase, and the dispersed seminiferous tubules were separated from the dissociated interstitial Leydig cells by gravity sedimentation through a Percoll cushion. The tubules were then digested with trypsin to single-cell suspensions. Next, Sertoli cells were separated from germ cells by filtration through a 40-μm cell strainer and by adhesion to lectin-coated culture plates. The germ cells were further resolved on a discontinuous Percoll gradient of 15, 22, 30, and 40% (Zhu et al., 2002). After centrifugation, cells were collected from the 15/22, 22/30, and 30/40 interfaces. Alternatively, the heterogeneous germ cells were resolved into four populations—spermatogonia, primary spermatocytes, secondary spermatocytes,

and spermatids—by a Hoechst dye-based flow cytometry approach (Bastos et al., 2005; Getun et al., 2011; Gaysinskaya et al., 2014). Briefly, following testis digestion (collagenase) and somatic cell removal (sedimentation), seminiferous tubules were further digested with collagenase/trypsin for 25 min at 35°C and prestained with Hoechst 33342 for 20 min. At the end of incubation, newborn calf serum was added to inactivate trypsin. After determining the cell number, the cell suspension was stained for 25 min by addition of Hoechst 33342 to the final concentration of 6 µg/million cells. Immediately before sorting, the cells were stained with propidium iodide and filtered through a 40-µm cell strainer. Fluorescence-activated cell sorting was performed on a 5-laser FACSaria IIu SORP cell sorter operated at the following wavelengths: 355, 407, 488, 561, and 633 nm. Approximately $0.5\text{--}2.0 \times 10^6$ cells were collected for each population. In separate experiments, we also collected nonadherent testicular cells without the use of proteases, using gentle mechanical agitation of minced seminiferous tubules in DMEM for 30 min at 37°C, which releases mostly spermatids as evidenced by Hoechst dye-based flow cytometry analysis.

Isolation of organelles from mouse testis

All procedures were performed on ice or in a cold room. Four decapsulated testes were homogenized in 12 ml isolation medium (0.28 M sucrose, 10 mM Tris, pH 7.4, and 0.25 mM EDTA) using a tight-fitting Teflon-glass homogenizer. The homogenate was spun at 700 *g* for 10 min. After that, the supernatant was spun at 8,000 *g* for 15 min. The post-8,000-*g* supernatant was spun at 16,000 *g* for 15 min, and the post-16,000-*g* supernatant was spun at 200,000 *g* for 1 h. All pellets were resuspended in isolation medium at a protein concentration of ~10 g/liter. Protein concentrations were determined by the Lowry procedure (Lowry et al., 1951). The post-8,000-*g* pellet was loaded onto a 30% Percoll solution in isolation medium and spun at 95,000 *g* for 30 min in a swing-out rotor. This step separated the membranes, rich in mitochondria, into a low-density and a high-density band. Those bands were collected and diluted 1:8 with isolation medium. Finally, the low- and high-density mitochondria were pelleted by centrifugation at 10,000 *g* for 20 min.

Condensed mitochondria were immuno-isolated from the low-density fraction of the 8,000-*g* pellet, and orthodox mitochondria were immuno-isolated from the high-density fraction of the 8,000-*g* pellet. The Mitochondria Isolation Kit (Miltenyi Biotec; 130-096-946) was used according to the manufacturer's instruction. Briefly, samples were incubated with anti-Tom22-coated microbeads. The monoclonal anti-Tom22 antibody specifically binds Tom22 of mouse mitochondria. Next, each sample was loaded onto a MACS column placed in the magnetic field of the MACS Separator, by which the microbeads and the bound mitochondria were retained on the column, whereas the unbound organelles were allowed to pass through. The magnetically retained mitochondria were eluted from the column after it was removed from the magnetic field. LNMs were collected by centrifugation from the flow-through of the low-density fraction. By using similar techniques with organelle-specific monoclonal antibodies and the µMACS Protein-G Microbeads (Miltenyi Biotec; 130-071-101),

other organelles, including late endosomes, endoplasmic reticulum, and the plasma membrane, were immuno-isolated. The organelle-specific mouse monoclonal antibodies included anti-IP3R-3 cytoplasmic domain (BD Biosciences; 610362) for endoplasmic reticulum, anti-Rab7 (Santa Cruz Biotechnology; 376362) for late endosomes, and anti-Na,K ATPase α-1 subunit (Abcam; ab7671) for the plasma membrane.

Preparation of acrosomal vesicles

The acrosomal membrane-enriched fraction was prepared as described (Stambouliau et al., 2005) with minor modifications. Briefly, sperm isolated from murine epididymis were capacitated in DMEM supplemented with BSA (20 mg/ml) and CaCl₂ (2 mM) for 45 min at 37°C. After centrifugation (500 *g*, 10 min) and resuspension in DMEM and CaCl₂ (2 mM) without BSA, the capacitated sperm were treated with the calcium ionophore A23187 (10 µM) for 30 min at 37°C to initiate the acrosome reaction. The postreaction sperm were collected by centrifugation of the reaction mixture for 5 min at 1,000 *g*, and the acrosomal vesicles released during the acrosome reaction were collected by centrifugation of the supernatant at 100,000 *g* for 1 h at 4°C.

Lipidomics

Lipids were extracted with chloroform and methanol as described (Bligh and Dyer, 1959). For the quantification of lipids, samples were spiked with internal standards at the first extraction step. These internal standards included the CL mix I, phosphatidylethanolamine 17:0/14:1, phosphatidylinositol 12:0/13:0, phosphatidylglycerol 12:0/13:0, sphingomyelin d18:1/12:0, and phosphatidylcholine 21:0/22:6. All standards were obtained from Avanti Polar Lipids. Lipid extracts were dried under nitrogen and then re-dissolved in chloroform:methanol 1:1. The re-dissolved extracts were analyzed by matrix-assisted laser desorption ionization time-of-flight (MALDI-TOF) MS (Fig. 1, b–f; Fig. 2, a, b, and e; Fig. 3 a; and Table S1), by LC-MS/MS (Fig. 1 a; Fig. 3, b–d; Fig. 5 d; Fig. S1 a; and Tables S2 and S3), or by LC-MSn (Fig. S1 b).

MALDI-TOF MS was performed as described (Sun et al., 2008). Aliquots of the lipid solutions were diluted 1:11 in 2-propanol-acetonitrile (3:2) and then mixed 1:1 with matrix solution containing 20 g/liter 9-aminoacridine in 2-propanol-acetonitrile (3:2). One microliter or less was applied onto the target spots, and MS was performed with a MALDI Micro MX mass spectrometer (Waters) operated in reflectron mode. The pulse voltage was set to 2,000 V, the detector voltage was set to 2,200 V, and the time-lag focusing delay was set to 700 ns. The nitrogen laser (337 nm) was fired at a rate of 5 Hz, and 10 laser shots were acquired per subspectrum. For the analysis of phosphatidylcholine and sphingomyelin, the instrument was operated in positive ion mode and for all other lipids in negative ion mode with a flight tube voltage of 12 kV, a reflectron voltage of 5.2 kV, and a negative anode voltage of 3.5 kV. The instrument was calibrated daily with polyethylene glycol fragments in positive ion mode, and with a reference mixture of lysophosphatidylglycerol 14:0 (*m/z* = 455.2415), phosphatidylglycerol 36:2 (*m/z* = 773.5338), phosphatidylethanolamine 36:2 (*m/z* = 738.5079), and CL 72:8 (*m/z* = 1,447.9650) in negative ion mode. We typically acquired 100–200 subspectra (representing

1,000–2,000 laser shots) per sample in a mass range from 400 to 2,000 D. Spectra were only acquired if their base peak intensity was within 10–95% of the saturation level. Uniform mass adjustment was performed with an internal reference mass. Data were analyzed with MassLynx 4.1 software.

LC-MS/MS and LC-MSn were performed with an LTQ Orbitrap (Thermo Fisher Scientific) coupled to an Ascentis Express C8 reversed-phase column (75 × 2.1 mm; 2.7 μm) from SUPELCO. Samples were injected by a 20-μl loop injector. A gradient was established by two conventional HPLC pumps run at a total flow rate of 0.1 ml/min. The gradient changed the solvent mixture 2-propanol/acetonitrile/water from 22.5/47.5/30 to 85.5/12.5/2 within 35 min under the continuous presence of 0.1% formic acid and 10 mM ammonium formate. The total run time was 90 min. The mass spectrometer was operated in negative ion mode by using the instrument settings established by the automated tuning program. Data were acquired in centroid mode from $m/z = 300$ to $m/z = 2,000$. The orbitrap (MS1) resolution was set to 60,000. MS2 data were acquired automatically with the collisional energy set to 40%. Data were analyzed with the software LipidSearch 4.1 (Thermo Fisher Scientific).

Proteomics

Sample proteins were concentrated by short SDS-PAGE runs into single-protein bands before tryptic digestion and peptide extraction. TMT-Labeling and the remaining proteomics protocols were performed by using methods previously described (Huang et al., 2017; Erdjument-Bromage et al., 2018) with the following modifications. TMT Label 129N, 129C, 130N, and 130C were added to each sample at a label:peptide ratio of 12:1 (wt/wt) and mixed briefly on a vortexer. The mixture was incubated at room temperature for 1 h, quenched by the addition of 10 μl 5% hydroxylamine, and then acidified by the addition of 10 μl 10% formic acid. A small aliquot from each reaction was desalted with Empore C18 High Performance Extraction Disks, and the eluted peptide solutions were partially dried under vacuum and then analyzed by LC-MS/MS with a Q Exactive High Field Orbitrap mass spectrometer to determine labeling efficiencies, which were found to be 98–99%. To ensure equal amounts of labeled peptides, samples were mixed and analyzed in test runs by LC-MS/MS. The final sample mixture containing mixed channels was prepared by adjusting the volume of individual samples so they contained equal amounts of labeled peptides. The mixture was desalted by using a Sep-Pak tC18 1 cc Vac Cartridge (Waters; WAT036820). Eluted peptides were subjected to triplicate analysis by using LC with a Thermo Easy nLC 1000 system coupled online to a Q Exactive HF with a NanoFlex source (Thermo Fisher Scientific) as previously described (Huang et al., 2017). All data were analyzed by the MaxQuant proteomics software (version 1.5.5.1) with the Andromeda search engine (Cox et al., 2011) by using a mouse database (mouse [*Mus musculus*] protein database; Uniprot; Reviewed, 16,950 entries, [12202017]). Reporter ion mass tolerance was set to 0.01 D, the activated precursor intensity fraction value was set to 0.75, and the false discovery rate was set to 1% for protein, peptide-spectrum match, and site decoy fraction levels. Peptides were required to have a minimum length of seven amino acids

and a mass no greater than 4,600 D. The reporter ion intensities were defined as intensities multiplied by injection time (to obtain the total signal) for each isobaric labeling channel summed over all MS/MS spectra as previously validated (Tyanova et al., 2016). We also performed separate analyses of unlabeled peptides by using the same LC-MS/MS method. Mass spectra were subjected to label-free quantitation by using MaxQuant proteomics data analysis workflow (version 1.5.5.1) with the Andromeda search engine (Cox et al., 2011; Tyanova et al., 2016).

Western blot analysis

Proteins were transferred from 10% SDS-PAGE gels to polyvinylidene difluoride membranes. The membranes were incubated in Odyssey blocking buffer with the following primary antibodies at a concentration of 1 μg/ml: rabbit polyclone antibody to sulfite oxidase from Invitrogen, mouse monoclonal antibody to α-subunit of ATP synthase from Abcam, rabbit monoclonal antibody to the receptor-binding cancer antigen 1 (Golgi marker) from Cell Signaling, and rabbit monoclonal antibody to protein disulfide isomerase (ER marker) from Cell Signaling. Fluorescent GAR-IDye800cw and GAM-IRDye680 secondary antibodies (1 μg/μl; LiCor) were used at a dilution of 1:15,000. Proteins were visualized and quantified by the LiCor scanner.

Quantitative EM

Samples were fixed in glutaraldehyde and osmium tetroxide. Fixed samples were stained with uranyl acetate. The buffer was gradually exchanged with ethanol, followed by resin exchange and heat polymerization. Sections of 50–100 nm were cut with a Leica Ultracut UCT microtome and collected on EM grids. Sections were stained with uranyl acetate and Sato Lead stains and imaged with a Philips CM12 transmission electron microscope. Random images were collected at different magnifications. Quantitative analysis was performed at a magnification of 7,100. Cells were categorized into spermatocytes, round spermatids, and elongated spermatids by the following criteria: (1) the general appearance, (2) the distance from the basal membrane, (3) the presence of an acrosome or a pro-acrosomal granule, and (4) the angle of the two lines extending from the center of the nucleus to the edges of the acrosome (Russel et al., 1990). Mitochondria were classified by the morphology of their matrix compartment as orthodox (compact matrix with narrow cristae), intermediate (fragmented matrix with wide cristae), and condensed (narrow matrix surrounding a single crista; De Martino et al., 1979).

Fluorescence and immunofluorescence microscopy

Fluorescence microscopy was performed on isolated non-adherent testicular cells (mostly spermatids) and epididymal sperm. Primary rabbit polyclonal antibodies to Ant4 (PA5-44133) and Suox (PA5-21705) were from Thermo Fisher Scientific. Primary antibodies to Spata18 (Ab180154) and SdhA (Ab14715) were from Abcam (Ab180154). Rat monoclonal anti-IZUMO1 antibody (125) was from AS ONE International. Fluorescent-labeled secondary antibodies, MitoTracker, Hoechst dye, and Antifade Mounting Media were purchased from Invitrogen. NAO was from Molecular Probes. Live cells in DMEM were stained with NAO (100 nM), MitoTracker Deep Red (100 nM), and Hoechst

34580 (0.2 $\mu\text{g/ml}$) for 30 min at 37°C according to published methods (Keij et al., 2000). After being washed three times with prewarmed DMEM, the stained cells were mounted in Antifade Live Mountant on the coverslip and imaged immediately with a Zeiss LSM 880 laser scanning confocal microscope. The NAO emission was captured in the red range, and the MitoTracker Deep Red emission was displayed in pseudo-color green. For immunofluorescence microscopy, cells in suspension were fixed in 3% paraformaldehyde for 30 min at room temperature and then washed with PBS by pelleting. Fixed cells were either processed for labeling in suspension or cytospun onto glass microscope slides before processing. Primary antibodies were applied according to the manufacturer's instructions, typically at a dilution of 1:200. Immunofluorescence images obtained without primary antibodies (secondary antibodies only) served as negative controls.

CL synthase activity

To prepare the substrates for CL synthase, 260 μl of CDP-diacylglycerol 18:1/18:1 in chloroform (0.962 mM; corresponding to 250 nmol) was mixed with 250 μl phosphatidylglycerol 14:0/14:0 in chloroform (1 mM; corresponding to 250 nmol). The solution was dried under nitrogen and then resuspended in 0.5 ml water by mechanical agitation and sonication. Samples of subcellular fractions were diluted to a protein concentration of 2 g/liter. An aliquot of 50 μl sample (0.1 mg protein) was mixed with 50 μl buffer (20 mM Tris, pH 7.4, at 37°C) and 5 μl 0.1 M CoCl_2 . The reaction was started by addition of 20 μl substrate, and the assay mixtures were incubated at 37°C for 1 h. The reaction was stopped by adding 2 ml methanol and 1 ml chloroform. This was followed by the addition of standard CL mixture I, containing 111 pmol CL 57:4, 101 pmol CL 61:1, 89 pmol CL 80:4, and 85 pmol CL 86:4. Lipids were extracted (Bligh and Dyer, 1959) and dried under nitrogen. The lipid extracts were re-dissolved in 0.1 ml chloroform:methanol 1:1 and analyzed by MALDI-TOF MS as described above. The amount of newly formed CL was quantified by measuring the intensity at $m/z = 1,347.9332$ (mass of CL 64:2 anion) and the intensities of the internal standards as reference. The amount of newly formed CL increased in a linear fashion from 50 to 150 μg of protein and from 30- to 90-min incubation time. The lower limit of detection was 1 pmol/min/mg protein. To apply this assay, it has to be verified that the mass spectrum does not contain endogenous signals within ± 3 D of $m/z = 1,348$.

Data and statistical analysis

Continuous variables are presented as mean values with the SEM. The number of replicas is given in the legends of the figures. Replicas refer to measurements made in separate animals. Mean values were compared by Student's *t* test or by ANOVA. Distributions between different types of mitochondria or cells were performed by the χ^2 test. For each genotype, the distribution data were collected from >30 electron micrographs prepared from four testes (two separate animals).

Online supplemental material

Fig. S1 shows mass spectra of TPCL in the testes of humans and mice. Fig. S2 shows the separation of germ cells by flow cytometry. Fig. S3 shows data indicating the presence of mitochondrially

annotated proteins in the acrosome. Fig. S4 shows immunofluorescence images of Suox and Spata18 in spermatids. Table S1 lists data from affinity purification experiments. Table S2 lists the lipid composition of acrosomal membranes. Table S3 lists CL molecular species in mitochondria and LNMs from mouse testis.

Acknowledgments

This work was supported in part by the National Institutes of Health (grant R01 GM115593 to M. Schlame, shared instrumentation grants RR027990 and S10OD023659, and core center grant NS050276 to T.A. Neubert).

The authors declare no competing financial interests.

Author contributions: M. Ren and M. Schlame conceived the study. M. Ren, Y. Xu, H. Erdjument-Bromage, C.K.L. Phoon, N. Terada, and M. Schlame performed the experiments and analyzed the data. A. Donelian performed the quantitative analysis of electron microscopy data. D. Strathdee developed the TAZ-KO mouse model. T.A. Neubert analyzed and interpreted the proteomics data. M. Schlame wrote the manuscript and secured funding. All authors edited the manuscript.

Submitted: 21 August 2018

Revised: 29 November 2018

Accepted: 7 March 2019

References

- Acehan, D., A. Malhotra, Y. Xu, M. Ren, D.L. Stokes, and M. Schlame. 2011. Cardiolipin affects the supramolecular organization of ATP synthase in mitochondria. *Biophys. J.* 100:2184–2192. <https://doi.org/10.1016/j.bpj.2011.03.031>
- Bastos, H., B. Lassalle, A. Chicheportiche, L. Riou, J. Testart, I. Allemand, and P. Fouchet. 2005. Flow cytometric characterization of viable meiotic and postmeiotic cells by Hoechst 33342 in mouse spermatogenesis. *Cytometry A*. 65A:40–49. <https://doi.org/10.1002/cyto.a.20129>
- Berruti, G. 2016. Towards defining an 'origin'—The case for the mammalian acrosome. *Semin. Cell Dev. Biol.* 59:46–53. <https://doi.org/10.1016/j.semcdb.2016.01.013>
- Beyer, K., and M. Klingenberg. 1985. ADP/ATP carrier protein from beef heart mitochondria has high amounts of tightly bound cardiolipin, as revealed by phosphorus-31 nuclear magnetic resonance. *Biochemistry*. 24:3821–3826. <https://doi.org/10.1021/bi00336a001>
- Bligh, E.G., and W.J. Dyer. 1959. A rapid method of total lipid extraction and purification. *Can. J. Biochem. Physiol.* 37:911–917. <https://doi.org/10.1139/y59-099>
- Brower, J.V., N. Rodic, T. Seki, M. Jorgensen, N. Fliess, A.T. Yachnis, J.R. McCarrey, S.P. Oh, and N. Terada. 2007. Evolutionarily conserved mammalian adenine nucleotide translocase 4 is essential for spermatogenesis. *J. Biol. Chem.* 282:29658–29666. <https://doi.org/10.1074/jbc.M704386200>
- Brower, J.V., C.H. Lim, M. Jorgensen, S.P. Oh, and N. Terada. 2009. Adenine nucleotide translocase 4 deficiency leads to early meiotic arrest of murine male germ cells. *Reproduction*. 138:463–470. <https://doi.org/10.1530/REP-09-0201>
- Brucker, C., and G.B. Lipford. 1995. The human sperm acrosome reaction: physiology and regulatory mechanisms. An update. *Hum. Reprod. Update*. 1:51–62. <https://doi.org/10.1093/humupd/1.1.51>
- Cadalbert, L.C., F.N. Ghaffar, D. Stevenson, S. Bryson, F.M. Vaz, E. Gottlieb, and D. Strathdee. 2015. Mouse tafazzin is required for male germ cell meiosis and spermatogenesis. *PLoS One*. 10:e0131066. <https://doi.org/10.1371/journal.pone.0131066>
- Chang, Y.-F., J.S. Lee-Chang, S. Panneerdoss, J.A. MacLean II, and M.K. Rao. 2011. Isolation of Sertoli, Leydig, and spermatogenic cells from the mouse testis. *Biotechniques*. 51:341–342. <https://doi.org/10.2144/000113764>
- Clarke, S.L., A. Bowron, I.L. Gonzalez, S.J. Groves, R. Newbury-Ecob, N. Clayton, R.P. Martin, B. Tsai-Goodman, V. Garratt, M. Ashworth, et al.

2013. Barth syndrome. *Orphanet J. Rare Dis.* 8:23. <https://doi.org/10.1186/1750-1172-8-23>
- Cox, J., N. Neuhauser, A. Michalski, R.A. Scheltema, J.V. Olsen, and M. Mann. 2011. Andromeda: a peptide search engine integrated into the MaxQuant environment. *J. Proteome Res.* 10:1794–1805. <https://doi.org/10.1021/pr101065j>
- De Martino, C., A. Floridi, M.L. Marcante, W. Malorni, P. Scorza Barcellona, M. Bellocchi, and B. Silvestrini. 1979. Morphological, histochemical and biochemical studies on germ cell mitochondria of normal rats. *Cell Tissue Res.* 196:1–22. <https://doi.org/10.1007/BF00236345>
- Dolce, V., P. Scarcia, D. Iacopetta, and F. Palmieri. 2005. A fourth ADP/ATP carrier isoform in man: identification, bacterial expression, functional characterization and tissue distribution. *FEBS Lett.* 579:633–637. <https://doi.org/10.1016/j.febslet.2004.12.034>
- Erdjument-Bromage, H., F.K. Huang, and T.A. Neubert. 2018. Sample Preparation for Relative Quantitation of Proteins Using Tandem Mass Tags (TMT) and Mass Spectrometry (MS). *Methods Mol. Biol.* 1741:135–149. https://doi.org/10.1007/978-1-4939-7659-1_11
- Gaysinskaya, V., I.Y. Soh, G.W. van der Heijden, and A. Bortvin. 2014. Optimized flow cytometry isolation of murine spermatocytes. *Cytometry A.* 85:556–565. <https://doi.org/10.1002/cyto.a.22463>
- Getun, I.V., B. Torres, and T.R.J. Bois. 2011. Flow cytometry purification of mouse meiotic cells. *J. Vis. Exp.* 50:2602.
- Horvath, S.E., and G. Daum. 2013. Lipids of mitochondria. *Prog. Lipid Res.* 52: 590–614. <https://doi.org/10.1016/j.plipres.2013.07.002>
- Huang, F.K., G. Zhang, K. Lawlor, A. Nazarian, J. Philip, P. Tempst, N. Dephore, and T.A. Neubert. 2017. Deep Coverage of Global Protein Expression and Phosphorylation in Breast Tumor Cell Lines Using TMT 10-plex Isobaric Labeling. *J. Proteome Res.* 16:1121–1132. <https://doi.org/10.1021/acs.jproteome.6b00374>
- Jiang, F., M.T. Ryan, M. Schlame, M. Zhao, Z. Gu, M. Klingenberg, N. Pfanner, and M.L. Greenberg. 2000. Absence of cardiolipin in the crdl null mutant results in decreased mitochondrial membrane potential and reduced mitochondrial function. *J. Biol. Chem.* 275:22387–22394. <https://doi.org/10.1074/jbc.M909868199>
- Keij, J.F., C. Bell-Prince, and J.A. Steinkamp. 2000. Staining of mitochondrial membranes with 10-nonyl acridine orange, MitoFluor Green, and MitoTracker Green is affected by mitochondrial membrane potential altering drugs. *Cytometry.* 39:203–210. [https://doi.org/10.1002/\(SICI\)1097-0320\(20000301\)39:3<203::AID-CYTOS>3.0.CO;2-Z](https://doi.org/10.1002/(SICI)1097-0320(20000301)39:3<203::AID-CYTOS>3.0.CO;2-Z)
- Kim, Y.-H., G. Haidl, M. Schaefer, U. Egner, A. Mandal, and J.C. Herr. 2007. Compartmentalization of a unique ADP/ATP carrier protein SFEC (Sperm Flagellar Energy Carrier, AAC4) with glycolytic enzymes in the fibrous sheath of the human sperm flagellar principal piece. *Dev. Biol.* 302:463–476. <https://doi.org/10.1016/j.ydbio.2006.10.004>
- Kitamura, N., Y. Nakamura, Y. Miyamoto, T. Miyamoto, K. Kabu, M. Yoshida, M. Futamura, S. Ichinose, and H. Arakawa. 2011. Mieap, a p53-inducible protein, controls mitochondrial quality by repairing or eliminating unhealthy mitochondria. *PLoS One.* 6:e16060. <https://doi.org/10.1371/journal.pone.0016060>
- Lewis, R.N.A.H., and R.N. McElhaney. 2009. The physicochemical properties of cardiolipin bilayers and cardiolipin-containing lipid membranes. *Biochim. Biophys. Acta.* 1788:2069–2079. <https://doi.org/10.1016/j.bbame.2009.03.014>
- Lim, C.H., J.V. Brower, J.L. Resnick, S.P. Oh, and N. Terada. 2015. Adenine nucleotide translocase 4 is expressed within embryonic ovaries and dispensable during oogenesis. *Reprod. Sci.* 22:250–257. <https://doi.org/10.1177/1933719114542026>
- Lowry, O.H., N.J. Rosebrough, A.L. Farr, and R.J. Randall. 1951. Protein measurement with the Folin phenol reagent. *J. Biol. Chem.* 193:265–275.
- Lu, Y.W., and S.M. Claypool. 2015. Disorders of phospholipid metabolism: an emerging class of mitochondrial disease due to defects in nuclear genes. *Front. Genet.* 6:3. <https://doi.org/10.3389/fgene.2015.00003>
- Meinhardt, A., B. Wilhelm, and J. Seitz. 1999. Mini symposium. New aspects of spermatogenesis. Expression of mitochondrial marker proteins during spermatogenesis. *Hum. Reprod. Update.* 5:108–119. <https://doi.org/10.1093/humupd/5.2.108>
- Mileykovskaya, E., and W. Dowhan. 2014. Cardiolipin-dependent formation of mitochondrial respiratory supercomplexes. *Chem. Phys. Lipids.* 179: 42–48. <https://doi.org/10.1016/j.chemphyslip.2013.10.012>
- Okabe, M. 2013. The cell biology of mammalian fertilization. *Development.* 140:4471–4479. <https://doi.org/10.1242/dev.090613>
- Perry, R.P., B. Thorell, L. Akerman, and B. Chance. 1959. Localization and assay of respiratory enzymes in single living cells. Absorbance measurements on the Nebenkern. *Nature.* 184:929–931. <https://doi.org/10.1038/184929a0>
- Ramalho-Santos, J., and S. Amaral. 2013. Mitochondria and mammalian reproduction. *Mol. Cell. Endocrinol.* 379:74–84. <https://doi.org/10.1016/j.mce.2013.06.005>
- Raposo, G., M.S. Marks, and D.F. Cutler. 2007. Lysosome-related organelles: driving post-Golgi compartments into specialisation. *Curr. Opin. Cell Biol.* 19:394–401. <https://doi.org/10.1016/j.ccb.2007.05.001>
- Ren, M., C.K. Phoon, and M. Schlame. 2014. Metabolism and function of mitochondrial cardiolipin. *Prog. Lipid Res.* 55:1–16. <https://doi.org/10.1016/j.plipres.2014.04.001>
- Rodić, N., M. Oka, T. Hamazaki, M.R. Murawski, M. Jorgensen, D.M. Maatouk, J.L. Resnick, E. Li, and N. Terada. 2005. DNA methylation is required for silencing of ant4, an adenine nucleotide translocase selectively expressed in mouse embryonic stem cells and germ cells. *Stem Cells.* 23:1314–1323. <https://doi.org/10.1634/stemcells.2005-0119>
- Russell, L.D., R.A. Ettlin, A.P.S. Hikim, and E.D. Clegg. 1990. *Histological and histopathological evaluation of the testis.* Cache River Press, Clearwater, FL.
- Sorice, M., A. Circella, R. Misasi, V. Pittoni, T. Garofalo, A. Cirelli, A. Pavan, G. M. Pontieri, and G. Valesini. 2000. Cardiolipin on the surface of apoptotic cells as a possible trigger for antiphospholipids antibodies. *Clin. Exp. Immunol.* 122:277–284. <https://doi.org/10.1046/j.1365-2249.2000.01353.x>
- Sorice, M., A. Circella, I.M. Cristea, T. Garofalo, L. Di Renzo, C. Alessandri, G. Valesini, and M.D. Esposti. 2004. Cardiolipin and its metabolites move from mitochondria to other cellular membranes during death receptor-mediated apoptosis. *Cell Death Differ.* 11:1133–1145. <https://doi.org/10.1038/sj.cdd.4401457>
- Stamboulis, S., M.-J. Moutin, S. Treves, N. Pochon, D. Grunwald, F. Zorzato, M. De Waard, M. Ronjat, and C. Arnould. 2005. Junctate, an inositol 1,4,5-triphosphate receptor associated protein, is present in rodent sperm and binds TRPC2 and TRPC5 but not TRPC1 channels. *Dev. Biol.* 286:326–337. <https://doi.org/10.1016/j.ydbio.2005.08.006>
- Sugiura, A., S. Mattie, J. Prudent, and H.M. McBride. 2017. Newly born peroxisomes are a hybrid of mitochondrial and ER-derived preperoxisomes. *Nature.* 542:251–254. <https://doi.org/10.1038/nature21375>
- Sun, G., K. Yang, Z. Zhao, S. Guan, X. Han, and R.W. Gross. 2008. Matrix-assisted laser desorption/ionization time-of-flight mass spectrometric analysis of cellular glycerophospholipids enabled by multiplexed solvent dependent analyte-matrix interactions. *Anal. Chem.* 80:7576–7585. <https://doi.org/10.1021/ac801200w>
- Tsuneki, M., Y. Nakamura, T. Kinjo, R. Nakanishi, and H. Arakawa. 2015. Mieap suppresses murine intestinal tumor via its mitochondrial quality control. *Sci. Rep.* 5:12472. <https://doi.org/10.1038/srep12472>
- Tyanova, S., T. Temu, and J. Cox. 2016. The MaxQuant computational platform for mass spectrometry-based shotgun proteomics. *Nat. Protoc.* 11: 2301–2319. <https://doi.org/10.1038/nprot.2016.136>
- Vreken, P., F. Valianpour, L.G. Nijtmans, L.A. Grivell, B. Plecko, R.J.A. Wanders, and P.G. Barth. 2000. Defective remodeling of cardiolipin and phosphatidylglycerol in Barth syndrome. *Biochem. Biophys. Res. Commun.* 279:378–382. <https://doi.org/10.1006/bbrc.2000.3952>
- Wang, H.-Y.J., S.N. Jackson, and A.S. Woods. 2007. Direct MALDI-MS analysis of cardiolipin from rat organs sections. *J. Am. Soc. Mass Spectrom.* 18:567–577. <https://doi.org/10.1016/j.jasms.2006.10.023>
- Wriessnegger, T., G. Gübitz, E. Leitner, E. Ingolic, J. Cregg, B.J. de la Cruz, and G. Daum. 2007. Lipid composition of peroxisomes from the yeast *Pichia pastoris* grown on different carbon sources. *Biochim. Biophys. Acta.* 1771: 455–461. <https://doi.org/10.1016/j.bbalip.2007.01.004>
- Xu, Y., C.K. Phoon, B. Berne, K. D'Souza, E. Hoedt, G. Zhang, T.A. Neubert, R. M. Epand, M. Ren, and M. Schlame. 2016. Loss of protein association causes cardiolipin degradation in Barth syndrome. *Nat. Chem. Biol.* 12: 641–647. <https://doi.org/10.1038/nchembio.2013>
- Zhang, J., Z. Guan, A.N. Murphy, S.E. Wiley, G.A. Perkins, C.A. Worby, J.L. Engel, P. Heacock, O.K. Nguyen, J.H. Wang, et al. 2011. Mitochondrial phosphatase PTPMT1 is essential for cardiolipin biosynthesis. *Cell Metab.* 13:690–700. <https://doi.org/10.1016/j.cmet.2011.04.007>
- Zhang, M., E. Mileykovskaya, and W. Dowhan. 2002. Gluing the respiratory chain together. Cardiolipin is required for supercomplex formation in the inner mitochondrial membrane. *J. Biol. Chem.* 277:43553–43556. <https://doi.org/10.1074/jbc.C200551200>
- Zhu, P.Y., Y.F. Huang, and J.P. Xu. 2002. [Isolation and identification of spermatids from mouse testis]. *Zhonghua Nan Ke Xue.* 8:28–31.
- Zinser, E., C.D. Sperka-Gottlieb, E.V. Fasch, S.D. Kohlwein, F. Paltauf, and G. Daum. 1991. Phospholipid synthesis and lipid composition of subcellular membranes in the unicellular eukaryote *Saccharomyces cerevisiae*. *J. Bacteriol.* 173:2026–2034. <https://doi.org/10.1128/jb.173.6.2026-2034.1991>